INSTITUTE OF PHYSICS PUBLISHING JOURNAL OF PHYSICS D: APPLIED PHYSICS
J. Phys. D: Appl. Phys. **38** (2005) 119–126 doi:10.1088/0022-3727/38/1/019

Improving reliability of modelling heat and fluid flow in complex gas metal arc fillet welds—part I: an engineering physics model

A Kumar, W Zhang and T DebRoy

Department of Materials Science and Engineering, The Pennsylvania State University, University Park, PA 16802, USA

Received 26 July 2004, in final form 16 November 2004
Published 16 December 2004
Online at stacks.iop.org/JPhysD/38/119

Abstract
Although numerical heat transfer and fluid flow models have provided significant insight about fusion welding processes and welded materials in recent years, several model input parameters cannot be easily prescribed from fundamental principles. As a result, the model predictions do not always agree with the experimental results. In order to address this problem, the approach adopted here is to develop and test a model that embodies a heat transfer and fluid flow sub-model and an algorithm for optimizing and learning the values of uncertain process variables from a limited volume of experimental data. The heat transfer and fluid flow sub-model numerically calculates three-dimensional temperature and velocity fields, the weld geometry and the shape of the solidified weld reinforcement surface during gas metal arc (GMA) welding of fillet joints. Apart from the transport of heat from the welding arc, additional heat from the metal droplets is also considered in the model. Alternative algorithms for optimization of uncertain welding variables are examined. The overall model is capable of estimating uncertain parameters such as the arc efficiency, effective thermal conductivity and effective viscosity from a limited number of data on weld geometry. Part I of this paper is focused on the details of the numerical model, optimization technique used and an examination of the important features of the model. In an accompanying article (part II), the application of the model to GMA fillet welding of mild steel is described.

1. Introduction

In the last decade, significant progress has been made in applying transport phenomena for obtaining a better understanding of complex fusion welding processes and welded materials [1–4]. For example, numerical calculations of heat transfer and fluid flow in welding have enabled accurate quantitative calculations of thermal cycles and fusion zone geometry in both gas tungsten arc [5] and laser welding [6]. In many simple systems, the computed thermal cycles have been used to quantitatively understand weld metal composition and phase composition [7, 8], grain structure [9, 10] and inclusion structure [11]. Numerical modelling of heat transfer and fluid flow has also been used to study the weld metal composition change owing to both evaporation of alloying elements [6] and dissolution of gases [12]. However, the numerical heat transfer and fluid flow codes for fusion welding have so far been used mostly by researchers rather than by practicing engineers [13–15]. There are several reasons for the restricted use of these advanced tools. An important difficulty is the uncertainty in specifying several input parameters of the model such as the arc efficiency. As a result, the computed results do not always match the experimental data. In order to overcome this difficulty, new models are needed that can assure correct prediction of temperature fields and fusion zone geometry.

The arc efficiency, the effective thermal conductivity and the effective viscosity of the liquid metal in the weld pool are the three important input parameters that cannot be easily specified [13–21]. Although the values of arc efficiency have been experimentally measured for many welding conditions, the reported values vary significantly even for apparently similar welding conditions, reflecting the complexity of the welding process. The values of the effective thermal conductivity and effective viscosity are important, since they allow accurate modelling of the high rates of transport of heat and mass in systems with strong fluctuating velocities that are inevitable in small weld pools with very strong convection currents [13–22]. Since fluctuating components of velocities exist in small weld pools with strong mean recirculating velocities, a common practice has been to consider an enhancement in the values of the liquid thermal conductivity and viscosity higher than their corresponding molecular values. Currently there is no fundamental basis for prescribing the effective thermal conductivity and effective viscosity in the weld pool based on scientific principles [13–15]. This work attempts to outline a modelling procedure utilizing the power of a numerical heat transfer and fluid flow model and an optimization algorithm to estimate these parameters as a function of power input. Due to the narrow range of the experimental data set, the variations of arc efficiency, effective thermal conductivity and effective viscosity are considered to be linear with input power.

The goal of this work is to estimate the variation of arc efficiency, effective thermal conductivity and effective viscosity with input power through a combination of an optimization algorithm, a heat transfer and fluid flow model and a set of experimentally measured weld pool penetration, throat and leg length. The optimization algorithm minimizes the error between the predicted and the experimentally observed penetration, throat and leg length during the gas metal arc (GMA) welding process by considering the sensitivity of these geometric parameters to each of the uncertain parameters. The Levenberg–Marquardt (LM) method and two versions of the conjugate gradient (CG) method, i.e. Fletcher–Reeves and Polak–Ribiere non-linear parameter optimization, are used to estimate these uncertain parameters with a well tested three-dimensional numerical heat and fluid flow model.

Due to the complexity of the problem, the work is divided into two parts: the numerical model and its application to fillet welding of mild steel. In this part (part I) of the paper, the salient features of the numerical heat transfer and fluid flow model and optimization modules are presented. Furthermore, the important features of the model are examined. An application of the model to investigating GMA parameters during fillet welding of A-36 mild steel is presented in part II.

2. Model description

2.1. Modelling of heat transfer and fluid flow during GMA fillet welding

The heat transfer and fluid flow model takes into account the liquid metal convection in the weld pool, the complex fillet joint geometry, the deformation of the weld pool top surface, additions of the filler metal and the heat transfer by metal droplets. The output from the model includes the temperature and velocity fields, thermal cycles, fusion zone geometry and solidified geometry of the weld reinforcement. Since, the numerical model of the heat transfer and fluid flow has been described in [1, 20, 21], only the salient features of the sub-model are summarized below.

2.1.1. Governing equations. By using a coordinate system attached to the heat source, the welding process can be treated as a steady state problem [1, 16, 17, 22]. Therefore, the heat transfer and fluid flow during welding can be calculated by solving the steady state continuity, momentum and energy conservation equations. For fillet welding, accurate solution of heat transfer and fluid flow with a deformable weld pool surface and complex joint geometry requires the use of a non-orthogonal deformable curvilinear grid system [16, 17]. Therefore, these governing equations are transformed from the Cartesian to the curvilinear coordinate system [16, 17]. The transformed governing equations are discretized using the control volume method, where the computational domain is divided into many small rectangular control volumes. Discretized equations for a variable are formulated by integrating the corresponding governing equation over the control volumes in the computational domain. A power law based scheme is used to describe the convective flux at the control volume faces [23]. A modified semi-implicit algorithm for pressure linked equations (SIMPLE) is used to solve the discretized equations.

2.1.2. Heat transfer from metal droplets. An important feature of the GMA welding is the finger penetration, which is mainly caused by the transfer of heat from the superheated metal droplets into the weld pool. In this work, the droplet heat transfer in the spray mode is effectively simulated by incorporating a time-averaged volumetric heat source term (S_v) in the energy conservation equation [1, 16, 24, 25].

2.1.3. Calculation of the weld pool top surface profile. During GMA fillet welding, the weld pool top surface under the electrode is depressed by the arc force. Furthermore, the addition of filler metal also deforms the weld pool. Therefore, the weld pool top surface is not flat and the surface profile needs to be determined. In this work, an energy minimization method was used. The total energy to be minimized includes the surface energy due to the change in area of the pool surface, the potential energy in the gravitational field and the work performed by the arc pressure displacing the pool surface. The arc pressure, P_a, is normally represented by a Gaussian distribution as

$$P_a = \frac{F}{2\pi\sigma_p^2} \exp\left(-\frac{x_h^2 + y_h^2}{2\sigma_p^2}\right), \tag{1}$$

where F is the total arc force, σ_p is the distribution parameter for arc pressure and x_h and y_h are the x and y distances to the arc axis, respectively. As shown in equation (1), the calculation of arc pressure distribution at the weld pool top surface requires knowledge of the total force and the distribution parameter.

The total arc force was calculated by integrating the measured arc pressure distribution data:

$$F = \int 2\pi r P'_a \, dr, \tag{2}$$

where P'_a is the measured arc pressure at a distance of r from the arc axis. Once the total arc force was obtained, the pressure distribution parameter was then determined by fitting [1, 16] the experimental distribution into equation (1).

The governing equations are solved simultaneously to obtain the temperature and velocity fields and the free surface profile. First, the modified SIMPLE algorithm is used to calculate the temperature and velocity fields [16, 17, 23]. Then, the free surface profile is calculated based on the temperature field obtained in the previous step. After the solution of the free surface profile, the z locations of the grids along the vertical direction are adjusted to fit the surface profile, and the temperature and velocity fields are then recalculated in the fitted grid system. The calculation procedure is repeated until converged temperature and velocity fields and the free surface profile are obtained. The physical property data of the A-36 mild steel [16, 17] used in the calculations are summarized in table 1. A 72 × 66 × 47 grid system was used and the corresponding solution domain had dimensions of 450 mm length, 108 mm width and 18 mm depth. Spatially non-uniform grids with finer grids near the heat source were used for maximum resolution of the variables. The calculations normally converged within 4000 iterations, which took about 12 min on a PC with 3.06 GHz Intel P4 CPU and 512 MB PC2700 DDR-SDRAM.

Table 1. Physical properties of the mild steel workpiece used in the calculation.

Physical property	Value
Liquidus temperature, T_L (K)	1785.0
Solidus temperature, T_S (K)	1745.0
Density of metal, ρ (kg m^{-3})	7200
Thermal conductivity of solid, k_S (J m^{-1} s^{-1}K^{-1})	21.0
Thermal conductivity of liquid, k_L (J m^{-1}s^{-1} K^{-1})	16.0
Specific heat of solid, c_{pS} (J kg^{-1} K^{-1})	703.4
Specific heat of liquid, c_p (J kg^{-1} K^{-1})	808.1
Surface tension of liquid metal (N m^{-1})	1.2
Viscosity of liquid metal, μ_L (kg m^{-1} s^{-1})	6.7×10^{-3}

Table 2. Welding conditions used in the experiments.

Case no	Contact tube to workpiece distance, CTWD (mm)	Wire feeding rate (mm s^{-1})	Welding speed (mm s^{-1})	Voltage (V)	Current (A)
1	22.2	169.3	4.2	31	312.0
2	22.2	211.7	6.4	31	362.0
3	22.2	169.3	6.4	33	312.0
4	22.2	211.7	4.2	33	362.0
5	28.6	169.3	6.4	31	286.8
6	28.6	169.3	4.2	33	286.8
7	28.6	211.7	4.2	31	331.4
8	28.6	211.7	6.4	33	331.4

2.2. Optimization of uncertain variables

2.2.1. The uncertain variables. The goal of the optimization problem is to determine how the uncertain parameters, e.g. arc efficiency, effective thermal conductivity and effective viscosity, vary with heat input per unit length. For simplicity we assume the following linear relations between these variables and heat input.

$$\eta = f_1 + f_2 \cdot P^*_e, \tag{3}$$

$$k_e = f_3 \cdot k_L + f_4 \cdot k_L \cdot P^*_i, \tag{4}$$

$$\mu_e = f_5 \cdot \mu_L + f_6 \cdot \mu_L \cdot P^*_i, \tag{5}$$

$$P^*_e = \frac{IV/(\pi r_w^2 w_f)}{\rho c_p (T_L - T_a) + \rho L}, \qquad P^*_i = \frac{IV/(\pi r_b^2 U_w)}{\rho c_p (T_L - T_a) + \rho L}, \tag{6}$$

where η is the arc efficiency, k_e the effective thermal conductivity, k_L the conductivity of the liquid material, μ_e the effective viscosity, μ_L the viscosity of the liquid material, I the current, V the voltage, r_w the wire radius, w_f the wire feeding rate, ρ the density, c_p the specific heat, T_L the liquidus temperature, T_a the ambient temperature, L the latent heat of the alloy, r_b the arc radius, U_w the welding speed and f_1, f_2, f_3, f_4, f_5 and f_6 are constants. In the literature, it has been shown that arc efficiency varies linearly with heat input per unit length but the slope of this variation depends on the welding conditions and the welding process [14, 15, 20, 24]. Recent work on butt welding showed that the effective thermal conductivity and effective viscosity are also linear functions of the heat input per unit length [14]. Also, due to the narrow range of the experimental data set used in this work, it is justified to use the linear variation of the arc efficiency, effective thermal conductivity and effective viscosity with input power. In equation (3), the input power is non-dimensionalized with the wire feeding rate and wire radius because if any of these two parameters is large more power will be consumed in wire melting. Therefore, less power will go to the workpiece from the arc. In the expressions of effective thermal conductivity and effective viscosity, the input power is non-dimensionalized with respect to the welding speed and the arc radius. At a high welding speed or the arc radius, the input power is distributed over a large area, which reduces the turbulence in the weld pool and lowers the effective thermal conductivity and viscosity. The values of η, k_e and μ_e calculated from equations (3), (4) and (5) can be used for the experimental conditions given in table 2 for GMA welding in the spray mode.

2.2.2. The optimization problem. In order to calculate the values of the arc efficiency, effective thermal conductivity and effective viscosity, we require values of constant terms, i.e. f_1, f_2, f_3, f_4, f_5 and f_6 in equations (3)–(5). To find the values of these terms, an objective function is minimized which depicts the difference between the computed and measured values [26–28]. For example, if the penetration, throat and leg length of the fusion zone are of interest, an objective function, O($\boldsymbol{f}$),

can be defined as follows:

$$O(\boldsymbol{f}) = \sum_{m=1}^{M}(p_m^e - p_m^c)^2 + \sum_{m=1}^{M}(t_m^e - t_m^c)^2 + \sum_{m=1}^{M}(l_m^e - l_m^c)^2, \tag{7}$$

where p_m^c, t_m^c and l_m^c are the computed penetration, actual throat and leg length of the weld bead, respectively, and p_m^e, t_m^e and l_m^e are the corresponding experimentally determined values of these three variables. The subscript m in equation (7) corresponds to a specific weld in a series of M number of total welds. In equation (7), $\boldsymbol{f}$ refers to a set of six uncertain non-dimensional parameters, f_1, f_2, f_3, f_4, f_5 and f_6, that are constant terms in the assumed linear functions of efficiency, η, effective thermal conductivity, k_e, and effective viscosity, μ_e, expressed by equations (3)–(5).

For the estimation of these uncertain variables, the LM method and two modifications of the CG method suggested by Fletcher–Reeves and Polak–Ribiere are used in this study. The mathematical descriptions of these techniques are available in various books [26–31], and the specific application of these methods for welding is described briefly in appendices A and B. A brief description of the main features of the calculations related to the welding problem is provided later.

The LM and the CG methods differ in the calculation of the step size, i.e. the increment in the uncertain parameter and the direction of descent, i.e. the relative change in the uncertain parameters. These methods require calculation of the partial derivatives of weld penetration, actual throat and leg length with respect to all six coefficients of uncertain parameters indicated in equations (3)–(5). These partial derivatives are generally referred to as the sensitivity of the computed weld penetration, actual throat and leg length with respect to the uncertain parameters [13–15, 26–31]. The values of these sensitivity terms are numerically computed from the heat transfer and fluid flow model. These sensitivity terms can be written in a matrix form, known as the sensitivity matrix, $[J]$. The elements of the sensitivity matrix, i.e. sensitivity coefficients, J_{ij}^k, are defined as:

$$J_{ij}^k = \frac{\partial (p_i^c)^k}{\partial f_j} + \frac{\partial (t_i^c)^k}{\partial f_j} + \frac{\partial (l_i^c)^k}{\partial f_j}$$
$$\text{where } i = 1 \text{ to } M \text{ and } j = 1 \text{ to } 6, \tag{8}$$

where k is the iteration number. The solution methodology is discussed briefly in the appendix.

3. Results and discussion

The calculated temperature and velocity fields and surface profile at various vertical longitudinal sections parallel to the welding direction for case #1 (table 2) are shown in figure 1, where the weld pool boundary is represented by the 1745 K solidus isotherm of the mild steel A-36. As shown in figure 1(*a*), the liquid metal motion is quite complicated due to the combined effects of the driving forces. In the middle of the weld pool, the liquid metal is driven downwards by the electromagnetic force, and a major anticlockwise circulation loop is formed along the central longitudinal plane, i.e. $Y = 0$ plane, as shown in figure 1(*a*). Behind this region, at the top surface of the weld pool, the Marangoni shear stress drives

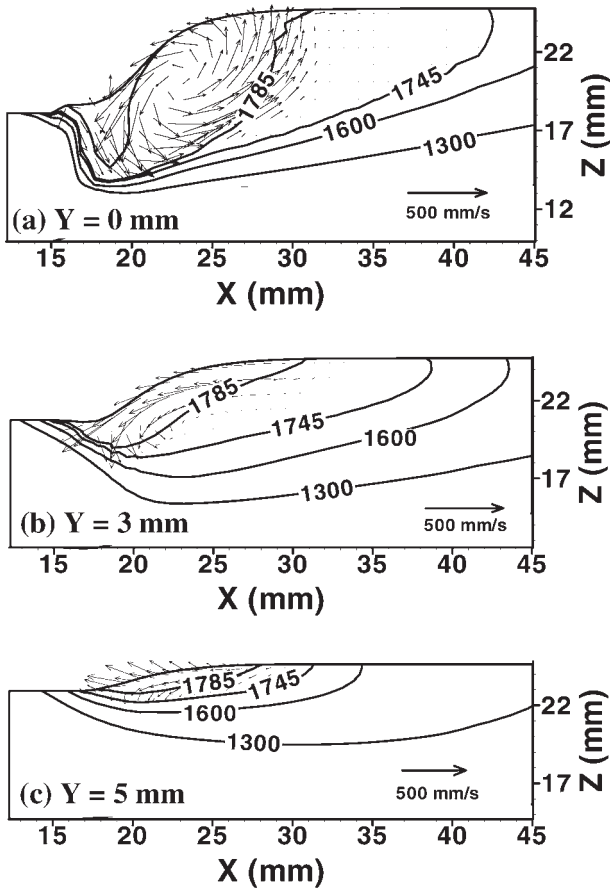

Figure 1. Calculated temperature and velocity vectors (shown by arrows) along various vertical longitudinal planes parallel to welding direction in a fillet weld. All the temperatures are given in Kelvin. The weld pool boundary is represented by the 1745 K isothermal line. The welding conditions are the same as those in case #1 in table 2.

the melt away from the middle to the edge of the pool. The region directly under the heat source is severely depressed under the effect of the arc pressure. As a result of the filler metal addition, the solidified weld metal forms a pronounced weld reinforcement. Figures 1(*b*) and (*c*) show that away from the heat source the weld pool surface shows considerably less depression, as would be expected from the reduction in arc pressure. Also, the peak temperatures are higher at locations close to the weld centre and decrease away from the heat source.

Figure 2 shows how the arc efficiency affects the computed weld dimensions. As expected, a higher arc efficiency results in larger weld dimensions because of the increase in heat input to the workpiece. All weld dimensions show a pronounced effect of arc efficiency. An opposite effect is observed in figure 3, where the effect of the effective thermal conductivity on the weld dimensions is examined. The increase in effective thermal conductivity, k_e, improves the heat transfer rate. More efficient heat distribution away from the heat source leads to smaller weld dimensions as shown in figure 3. Figure 4 shows that the weld pool dimensions do not change significantly with an increase in μ_e. This is due to the fact that the weld dimensions are mainly dependent on the absorbed power and other factors such as the droplet temperature, frequency

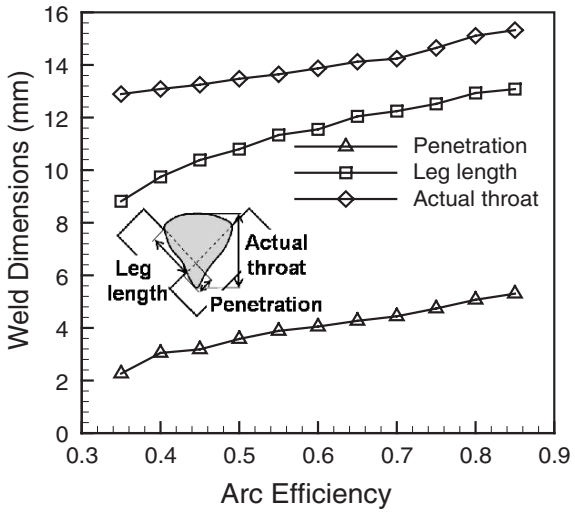

Figure 2. Variation of the weld pool dimensions with arc efficiency. The welding conditions are the same as those in case #1 in table 2.

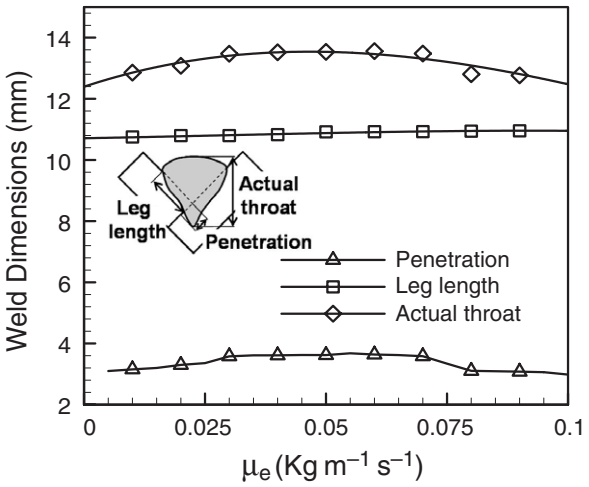

Figure 4. Variation of the weld pool dimensions with effective viscosity, μ_e. The welding conditions are the same as those in case #1 in table 2.

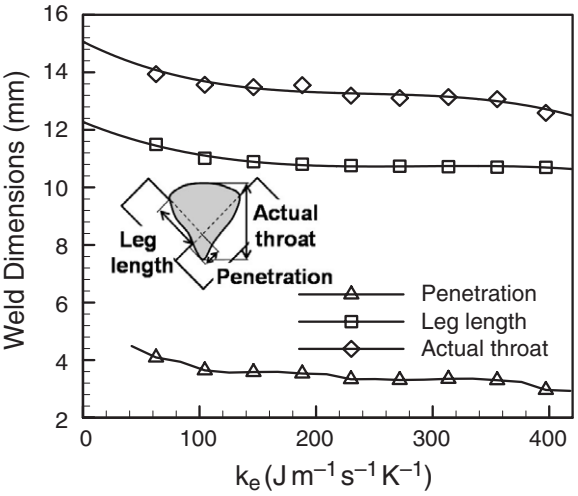

Figure 3. Variation of the weld pool dimensions with effective thermal conductivity, k_e. The welding conditions are the same as those in case #1 in table 2.

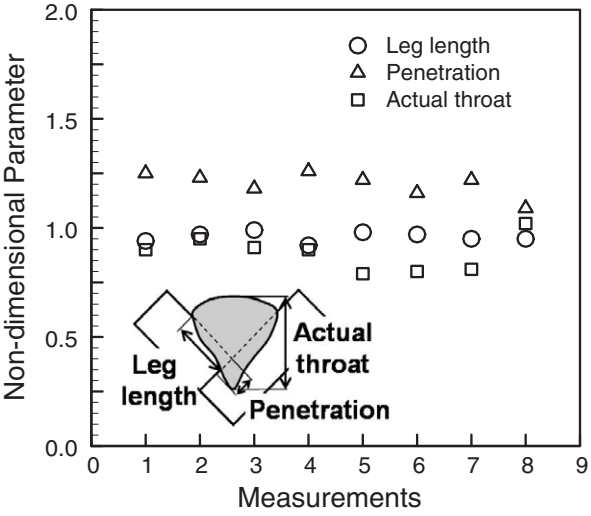

Figure 5. Computed values of non-dimensional actual throat, penetration and leg length using $\eta = 0.59$, $k_e = 209.0\,\mathrm{J\,m^{-1}\,s^{-1}\,K^{-1}}$ and $\mu_e = 0.12\,\mathrm{kg\,m^{-1}\,s^{-1}}$ for all the eight measurement cases listed in table 2. The non-dimensional values of penetration, actual throat and leg length are obtained by dividing their computed values with the corresponding experimentally measured values.

and welding speed. The droplet radius and droplet frequency significantly affect the dimensions of the actual throat and penetration, whereas the leg length is influenced by the arc radius and the input power. The trends shown in figures 2, 3 and 4 are also true for other values of current, voltage, wire feed rate, CTWD and welding speed.

Figure 5 shows the non-dimensional penetration, actual throat and leg length obtained by using values of arc efficiency of 0.54, $k_e = 209.0\,\mathrm{J\,m^{-1}\,s^{-1}\,K^{-1}}$ and $\mu_e = 0.12\,\mathrm{kg\,m^{-1}\,s^{-1}}$ as suggested in [18–21, 24]. The non-dimensional penetration value obtained using these values are higher than 1.0 for most of the cases. Therefore, the suggested combination of μ_e and k_e will not lead to optimum prediction of geometry for the weld conditions studied here, and a set of optimized values of η, μ_e and k_e is needed.

The following tasks were undertaken to examine the effectiveness of the optimization scheme:

(a) The heat transfer and fluid flow calculations were done with a set of assumed values of η, μ_e and k_e of 0.6, $0.064\,\mathrm{kg\,m^{-1}\,s^{-1}}$ and $80.0\,\mathrm{J\,m^{-1}\,s^{-1}\,K^{-1}}$, respectively, to calculate the leg length, penetration and actual throat for the welding conditions pertinent to cases #1, #3, #7 and #8 in table 2. These cases were selected because of the similarity of the welding conditions, so that the same values of arc efficiency, effective thermal conductivity and effective viscosity are appropriate for all the four cases.

(b) In order to check if the optimization model is capable of determining the correct values of uncertain welding parameters, the computed values of leg length, penetration and actual throat calculated in step (a) for the four cases were used as known geometric parameters. The model should be able to predict the same values of η, μ_e and k_e as assumed in step (a). To start the calculations, a set of initial values of these parameters were deliberately chosen to be different from the values used in step (a). The starting values of $\eta = 0.75$,

Table 3. Estimates of the exact parameters (i.e. $\eta = 0.6$, $k_e = 80.0\,\mathrm{J\,m^{-1}\,s^{-1}\,K^{-1}}$, $\mu_e = 0.064\,\mathrm{kg\,m^{-1}\,s^{-1}}$) during validation of the model by using the LM method and two versions of the CG method, i.e. Fletcher–Reeves and Polak–Ribiere, using initial assumed values of $\eta = 0.75$, $k_e = 63.0\,\mathrm{J\,m^{-1}\,s^{-1}\,K^{-1}}$ and $\mu_e = 0.0512\,\mathrm{kg\,m^{-1}\,s^{-1}}$.

		Error, i.e. $\sigma = 0.0$ mm		Error, i.e. $\sigma = 0.2$ mm	
Technique	Parameters	Estimates	Confidence interval	Estimates	Confidence interval
LM	η	0.602	—	0.610	$0.591 \leqslant \eta \leqslant 0.629$
	k_e ($\mathrm{J\,m^{-1}\,s^{-1}\,K^{-1}}$)	82.011	—	82.602	$78.684 \leqslant k_e \leqslant 86.524$
	μ_e ($\mathrm{kg\,m^{-1}\,s^{-1}}$)	0.063	—	0.064	$0.059 \leqslant \mu_e \leqslant 0.069$
Fletcher–Reeves CG	η	0.601	—	0.609	$0.595 \leqslant \eta \leqslant 0.623$
	k_e ($\mathrm{J\,m^{-1}\,s^{-1}\,K^{-1}}$)	81.259	—	80.159	$77.218 \leqslant k_e \leqslant 83.098$
	μ_e ($\mathrm{kg\,m^{-1}\,s^{-1}}$)	0.063	—	9.934	$0.060 \leqslant \mu_e \leqslant 0.068$
Polak–Ribiere CG	η	0.602	—	0.611	$0.598 \leqslant \eta \leqslant 0.624$
	k_e ($\mathrm{J\,m^{-1}\,s^{-1}\,K^{-1}}$)	81.268	—	80.241	$76.912 \leqslant k_e \leqslant 83.572$
	μ_e ($\mathrm{kg\,m^{-1}\,s^{-1}}$)	0.063	—	0.063	$0.059 \leqslant \mu_e \leqslant 0.069$

$\mu_e = 0.0512\,\mathrm{kg\,m^{-1}\,s^{-1}}$ and $k_e = 63.0\,\mathrm{J\,m^{-1}\,s^{-1}\,K^{-1}}$ were used to search for the optimized values of these three quantities.

(c) The objective function was then calculated using equation (7) and the computed values of leg length, penetration and actual throat obtained in step (a). This computed objective function was minimized by adjusting the values of η, μ_e and k_e using the optimization methods discussed in this paper. The obtained optimized values of η, μ_e and k_e were compared with those used in step (a) and presented in table 3.

All the three optimization techniques gave converged solutions within seven iterations as evidenced by the low values of the objective function, smaller than $10^{-6}\,\mathrm{m^2}$. Table 3 shows that almost exact values of all three parameters are obtained from all the optimization techniques. Thus, the optimization techniques can provide correct values of η, μ_e and k_e when the weld dimensions are known.

In reality, weld dimensions may vary from run to run for the same welding conditions because of random measurement errors. To simulate this variation and examine how the random errors in the measurements would affect the optimization process, random errors were introduced in the values of leg length, penetration and actual throat obtained from step (a) by adding appropriate error terms to the weld dimensions in the following manner [27]:

$$p = p_{ex} + \omega_1\sigma, \tag{9a}$$

$$t = t_{ex} + \omega_2\sigma, \tag{9b}$$

$$l = l_{ex} + \omega_3\sigma, \tag{9c}$$

where the subscript 'ex' means exact dimension obtained in step (a), σ is the standard deviation in these dimensions and ω_1, ω_2 and ω_3 are random variables with normal distribution, zero mean and unitary standard deviation. It may be noted from equation (9) that the same magnitude of errors was added to the penetration, leg length and actual throat since the measurement errors were experimentally found to be roughly equal. The value of σ was taken as 0.2 mm based on analysis of experimental data, and the Box–Miller method [27, 32] was used to generate the three random numbers, ω_1, ω_2 and ω_3. The values of penetration, actual throat and leg length obtained from equation (9) represent the region where the actual values of these variables will lie for a known value of the variance and probability (or confidence limit). For the 95% confidence level [27], ω_1, ω_2 and ω_3 lie between -1.96 and $+1.96$. Consequently, the values of penetration, leg length and actual throat lie between their values calculated in step (a) $\pm 1.96\sigma$ with a probability of 0.95. The results in table 3 indicate that when the weld dimensions contain random errors, accurate estimates of η, μ_e and k_e can be obtained by all three gradient based methods using starting values of $\eta = 0.75$, $\mu_e = 0.0512\,\mathrm{kg\,m^{-1}\,s^{-1}}$ and $k_e = 63.0\,\mathrm{J\,m^{-1}\,s^{-1}\,K^{-1}}$. As the errors introduced in equation (9) are Gaussian in distribution, the accuracy of the calculated values of η, μ_e and k_e can be checked by calculating the standard deviation of their values. The confidence intervals of η, μ_e and k_e obtained from the covariance matrix and given in table 3 show that the original values of these parameters lie in the range predicted by the proposed model for the 95% confidence level. These results show that the proposed model is able to capture the values of η, μ_e and k_e accurately when the measurements of geometrical dimensions contain random errors.

4. Summary and conclusions

To improve the reliability of numerical heat transfer and fluid flow calculations, a comprehensive model has been developed and tested that embodies a heat transfer and fluid flow sub-model and an algorithm for searching and optimizing the values of uncertain process variables from a limited volume of experimental data. The model was used to estimate the values of three parameters, arc efficiency (η), effective thermal conductivity (k_e) and viscosity (μ_e), as a function of the welding conditions. The numerical heat transfer and fluid flow model can capture the main geometric characteristics of fillet weld beads. In particular, the characteristic shape of finger penetration and weld reinforcement can be reasonably calculated considering the volumetric heat source, droplet addition and free surface deformation. The numerical heat transfer and fluid flow model was used to study the effect of η, μ_e and k_e on the fusion zone dimensions. It is found that the fusion zone dimensions increase with an increase in arc efficiency and decrease with a increase in the value of the effective thermal conductivity. The effective viscosity has much less effect on the fusion zone dimensions than do the other two parameters. It is shown that the values of the uncertain welding parameters can be determined from

the proposed method even when the measurements contain random errors.

Acknowledgments

The authors thank Dr C H Kim for useful discussions and S Mishra and X He for their useful comments on the manuscript. This research was supported by a grant from the US Department of Energy, Office of Basic Energy Sciences, Division of Materials Sciences, under grant no DE-FGO2-01ER45900.

Appendix A. LM method

The following equation was used to determine the uncertain parameters using the LM method:

$$([S]^k + \lambda^k \Omega^k)\{\Delta f^k\} = \{S^*\}^k, \tag{A.1}$$

where $[S]^k$ is a 6×6 matrix containing sensitivity terms, Δf^k is a 6×1 matrix, $\{S^*\}^k$ is a 6×1 matrix, λ^k is a scalar damping coefficient and is usually taken as 0.001 and $[\Omega^k]$ is the diagonal matrix. The order of $[\Omega^k]$ is the same as that of the matrix $[S]^k$ and is defined as $[\Omega^k] = \text{diag}[S]^k$. The elements of the matrices $[S]^k$ and $\{S^*\}^k$, i.e. S^k_{ij} and $(S^*_i)^k$, can be written as

$$S^k_{ij} = \sum_{m=1}^{M} \left(\frac{\partial (p^c_m)^k}{\partial f_i} \frac{\partial (p^c_m)^k}{\partial f_j} + \frac{\partial (t^c_m)^k}{\partial f_i} \frac{\partial (t^c_m)^k}{\partial f_j} + \frac{\partial (l^c_m)^k}{\partial f_i} \frac{\partial (l^c_m)^k}{\partial f_j} \right) \quad \text{for } i, j = 1 \text{ to } 6, \tag{A.2}$$

$$(S^*_i)^k = \sum_{m=1}^{M} \left(\{p^e_m - (p^c_m)^k\} \frac{\partial (p^c_m)^k}{\partial f_i} + \{t^e_m - (t^c_m)^k\} \frac{\partial (t^c_m)^k}{\partial f_i} + \{l^e_m - (l^c_m)^k\} \frac{\partial (l^c_m)^k}{\partial f_i} \right) \quad \text{for } i = 1 \text{ to } 6. \tag{A.3}$$

The elements of matrix $\{\Delta f^k\}$, i.e. Δf^k_i, calculated using equations (A.1)–(A.3) are used to calculate the values of uncertain variables at the next iteration.

$$f^{k+1}_i = f^k_i + \Delta f^k_i \qquad \text{for } i = 1 \text{ to } 6. \tag{A.4}$$

The parameter λ^k is then gradually decreased as the iteration procedure advances to the solution of the parameter estimation problem [15, 26–30].

Appendix B. CG method

The specific algorithm used for the minimization of the objective function based on the CG method is given by the following equation:

$$f^{k+1}_i = f^k_i - \beta^k d^k_i \qquad \text{for } i = 1 \text{ to } 6, \tag{B.1}$$

where β^k is the search step size, k the number of iterations and d^k_i is the direction of descent for the ith variable, which is a conjugation of the its gradient direction, $\nabla O(f^k)_i$, and its direction of descent in the previous iteration, d^{k-1}_i, and is given as

$$d^k_i = [\nabla O(f^k)]_i + \gamma^k d^{k-1}_i \qquad \text{for } i = 1 \text{ to } 6, \tag{B.2}$$

where γ^k is the conjugation coefficient. Different expressions are available in the literature for the conjugate coefficient, γ^k. Fletcher and Reeves [31] suggested

$$\gamma^k = \frac{\sum_{i=1}^{6} [\nabla O(f^k)]^2_i}{\sum_{i=1}^{6} [\nabla O(f^{k-1})]^2_i} \quad \text{for } k = 1, 2, \ldots \quad \text{and} \quad \gamma^0 = 0. \tag{B.3}$$

Polak–Ribiere [30] suggested this expression for γ^k:

$$\gamma^k = \frac{\sum_{i=1}^{6} [\nabla O(f^k)]_i [\nabla O(f^k) - \nabla O(f^{k-1})]_i}{\sum_{i=1}^{6} [\nabla O(f^{k-1})]^2_i} \quad \text{for } k = 1, 2, \ldots \quad \text{and } \gamma^0 = 0. \tag{B.4}$$

The search step size, β^k, is obtained as the one which minimizes the objective function and can be written as

$$\beta^k = \sum_{m=1}^{M} \left\{ (p^c_m - p^e_m) \left[\sum_{i=1}^{6} \left(\frac{\partial p^c_m}{\partial f^k_i} \right) d^k_i \right] + (t^c_m - t^e_m) \left[\sum_{i=1}^{6} \left(\frac{\partial t^c_m}{\partial f^k_i} \right) d^k_i \right] + (l^c_m - l^e_m) \times \left[\sum_{i=1}^{6} \left(\frac{\partial l^c_m}{\partial f^k_i} \right) d^k_i \right] \right\} \left\{ \sum_{m=1}^{M} \left[\sum_{i=1}^{6} \left(\frac{\partial p^c_m}{\partial f^k_i} \right) d^k_i + \sum_{i=1}^{6} \left(\frac{\partial t^c_m}{\partial f^k_i} \right) d^k_i + \sum_{i=1}^{6} \left(\frac{\partial l^c_m}{\partial f^k_i} \right) d^k_i \right]^2 \right\}^{-1}. \tag{B.5}$$

After computing the sensitivity terms, the gradient direction, the conjugation coefficient and the search step size, the iterative procedure given by equation (B.1) is implemented until a stopping criterion is satisfied.

References

[1] Kim C H, Zhang W and DebRoy T 2003 *J. Appl. Phys.* **94** 2667
[2] David S A and DebRoy T 1992 *Science* **257** 497
[3] DebRoy T and David S A 1995 *Rev. Mod. Phys.* **67** 85
[4] DebRoy T 2003 *Indian Weld. J.* **36** 59
[5] Zhang W, Roy G, Elmer J W and DebRoy T 2003 *J. Appl. Phys.* **93** 3022
[6] He X, DebRoy T and Fuerschbach P W 2003 *J. Appl. Phys.* **94** 6949
[7] Elmer J W, Palmer T A, Zhang W, Wood B and DebRoy T 2003 *Acta Mater.* **51** 3333
[8] Zhang W, Elmer J W and DebRoy T 2002 *Mater. Sci. Eng.* A **333** 321
[9] Mishra S and DebRoy T 2004 *Acta Mater.* **52** 1183
[10] Sista S and DebRoy T 2001 *Metall. Mater. Trans.* B **32** 1195
[11] Hong T and DebRoy T 2003 *Metall. Mater. Trans.* B **34** 267
[12] David S A, Trivedi R, Eshelman M E, Vitek J M, Babu S S, Hong T and DebRoy T 2003 *J. Appl. Phys.* **93** 4885
[13] De A and DebRoy T 2004 *J. Phys. D: Appl. Phys.* **37** 140
[14] De A and DebRoy T 2004 *J. Appl. Phys.* **95** 5230
[15] Kumar A and DebRoy T 2004 *Int. J. Heat Mass Tranfer* **47** 5789
[16] Zhang W, Kim C H and DebRoy T 2004 *J. Appl. Phys.* **95** 5210
[17] Zhang W, Kim C H and DebRoy T 2004 *J. Appl. Phys.* **95** 5220
[18] Hong K, Weckmann D C, Strong A B and Zheng W 2002 *Sci. Technol. Weld. Joining* **7** 125
[19] Jonsson P G, Szekely J, Choo R T C and Quinn T P 1994 *Modelling Simul. Mater. Sci. Eng.* **2** 995
[20] Hong K, Weckman D C, Strong A B and Pardo E 1992 *Proc. Ist Int. Conf. on Transport Phenomena in Processing (Hawaii)* ed S I Guceri (Technomic) p 626
[21] Choo R T C and Szekely J 1994 *Weld. J.* **73** 25

[22] Mundra K, DebRoy T and Kelkar K M 1996 *Numer. Heat Transfer* A **29** 115
[23] Patankar S V 1982 *Numerical Heat Transfer and Fluid Flow* (New York: McGraw-Hill)
[24] Lancaster J F 1986 *The Physics of the Welding* (Oxford: Pergamon)
[25] Kumar S and Bhaduri S C 1994 *Metall. Trans.* B **25** 435
[26] Beck J V, Blackwell B and St Clair C R 1985 *Inverse Heat Conduction: Ill-Posed Problems* (New York: Wiley)
[27] Ozisik M N and Orlande H R B 2002 *Inverse Heat Transfer: Fundamentals and Applications* (New York: Taylor and Francis)
[28] Beck J V and Arnold K J 1977 *Parameter Estimation in Engineering and Science* (New York: Wiley)
[29] Bard Y 1974 *Nonlinear Parameter Estimation* (New York: Academic)
[30] Dennis J and Schnabel R 1996 *Numerical Methods for Unconstrained Optimizations and Non-Linear Equations* (Philadelphia: SIAM)
[31] Fletcher R and Reeves C M 1964 *Comput. J.* **7** 149
[32] Press W H, Flannery B P, Teukolsky S A and Vetterling W T 1988 *Numerical Recipes* (Cambridge: Cambridge University Press)